Spectroscopy of tetragonal Eu:NaGd(WO_4)$_2$ crystal

P.A. Loiko[1,2], E.V. Vilejshikova[1], X. Mateos[2,*], J.M. Serres[2],
V.I. Dashkevich[3], V.A. Orlovich[3], A.S. Yasukevich[1], N.V. Kuleshov[1],
K.V. Yumashev[1], S.V. Grigoriev[1], S.M. Vatnik[4], S.N. Bagaev[4],
and A.A. Pavlyuk[5]

[1]Center for Optical Materials and Technologies (COMT), Belarusian National Technical University, 65/17 Nezavisimosti Ave., Minsk 220013, Belarus, e-mail: kinetic@tut.by
[2]Física i Cristal·lografia de Materials i Nanomaterials (FiCMA-FiCNA), Universitat Rovira i Virgili (URV), Campus Sescelades, c/ Marcel·lí Domingo, s/n., Tarragona, Spain E-43007
[3]B.I. Stepanov Institute of Physics, National Academy of Sciences of Belarus, 68 Nezavisimosti Ave., Minsk, Belarus 220072
[4]Institute of Laser Physics, Siberian Branch of Russian Academy of Sciences, 13/3 Lavrentyev Ave., Novosibirsk, Russia 630090
[5]A.V. Nikolaev Institute of Inorganic Chemistry, Siberian Branch of Russian Academy of Sciences, 3 Lavrentyev Ave., Novosibirsk, Russia 630090

*Corresponding author, e-mail: xavier.mateos@urv.cat

Abstract We report on growth and detailed spectroscopic study of Eu^{3+}-doped tetragonal sodium gadolinium double tungstate, Eu:NaGd(WO_4)$_2$, a new promising crystal for deep-red lasers. Large-volume crystal doped with 4.9 at.% Eu is grown by Czochralski method along the [001] crystallographic direction. Absorption of Eu^{3+} ions is studied at room temperature (RT) and at 6 K. For the absorption band related to the $^7F_1 \rightarrow {}^5D_1$ transition suitable for pumping of Eu:NaGd(WO_4)$_2$, the maximum cross-section is $\sigma_{abs} = 1.2\times10^{-21}$ cm^2 at 535.5 nm with the full width at half maximum (FWHM) of 3.1 nm (at RT, for $E \parallel a$ polarization). For the $^5D_0 \rightarrow {}^7F_4$ transition, the maximum stimulated-emission cross-section is $\sigma_{SE} = 1.6\times10^{-21}$ cm^2 at 698.3 nm (RT, $E \parallel c$ polarization). Lifetime of the $^5D_0$ state is 490±10 μs (at RT). Under UV excitation, Eu:NaGd(WO_4)$_2$ provides intense red emission with CIE coordinates ($x = 0.671$, $y = 0.329$).

Keywords: double tungstates, europium, absorption, luminescence

1. Introduction

Tetragonal sodium double tungstates (DT) and double molybdates (DMo) have the common chemical formula $Na^{+}R^{3+}(T^{6+}O^{2-}{}_4)_2$ where R = Gd, Y, Lu, La or Bi and T = W (for DT) or Mo (for DMo), when doped with trivalent rare-earth ions, are promising materials for solid-state lasers emitting in the near-IR [1-5]. In particular, efficient laser operation with Nd^{3+} [6], Yb^{3+} [7,8], Tm^{3+} [9,10] and Ho^{3+} ions [11] has been reported. These materials have an important advantage as compared with their monoclinic counterparts where Na^{+} is replaced by K^{+}, i.e. the absence of polymorph phase transition [12], so they can be easily grown by the Czochralski method [13,14]. Sodium DT and DMo normally have a scheelite-like structure. For scheelite, $CaWO_4$, (space group $C^6_{4h} \equiv I4_1/a$), Ca^{2+} has strongly distorted dodecahedral local environment by O^{2-} ions (local symmetry S_4) and W^{6+} ions are located in the center of distorted oxygen tetrahedron. In sodium scheelite-like DT and DMo, Na^{+} and R^{3+} ions can be distributed among Ca^{2+} positions statistically, partially or fully ordered [2,13]. This disorder leads to locally variable crystal field acting on the dopant ion which is expressed in the large bandwidth of the spectral lines. Particularly this has determined the interest to tetragonal DT and DMo for the use in femtosecond lasers [15,16].

Eu^{3+} ion is attractive due to intense red emission. It originates from the radiative transitions from the metastable $^5D_0$ state to the lower-lying ^7F_J (J = 0...6) multiplets. As the energy gap between the $^5D_0$ state and lower-lying excited-state is rather large, > 12000 cm^{-1}, quantum efficiency for the luminescence from this multiplet is approaching unity. Red Eu^{3+} luminescence is used in red and orange-red phosphors like the commercial yttrium oxide, $Eu:Y_2O_3$ [17], for applications in tricolour lamps, field emission displays, cathode-ray tubes and solid-state lighting [18-21]. Eu^{3+} ion provides also the possibilities for laser operation in the red (~610 nm, $^5D_0 \rightarrow {}^7F_2$ transition) [22,23] and deep-red (~700 nm, $^5D_0 \rightarrow {}^7F_4$) regions [24]. Such red lasers can be potentially used in medicine. To date, the interest for DT and DMo doped with Eu^{3+} ions was focused on their photoluminesent properties for potential phosphor applications. In this way, tetragonal [25-28] and monoclinic [29-32] materials were studied in the form of nano-powders. In particular, Eu-doped sodium DT and DMo, as well as their solid solutions which are possible due to close ionic radii of W^{6+} and Mo^{6+}, have provided intense emission in the red under UV excitation.

Laser action was achieved with monoclinic potassium double tungstates, $Eu:KRE(WO_4)_2$ or K*RE*W with *RE* = Gd [33] and Y [34] and the feasibility of laser operation with Eu:KLuW was also discussed [35]. However, power scaling of those lasers was limited due to the low pumping efficiency resulting from narrow absorption bands and limited crystal size. These drawbacks can be overcome by using tetragonal sodium DT which can offer broad spectral bands together with easy Czochralski growth of large bulk samples. For Eu^{3+} doping, $NaGd(WO_4)_2$ crystal or shortly NGW seems to be very suitable due to closeness of ionic radii of VIII-fold oxygen-coordinated Gd^{3+} (R_{ion} = 1.053 Å) and Eu^{3+} (R_{ion} = 1.066 Å). Thus, the aim of the present paper was to grow large-volume Eu:NGW crystals and to study their spectroscopic properties relevant for laser operation (i.e., transition cross-sections and lifetime of the emitting state).

2. Crystal growth

The studied Eu:NGW crystal was grown by the conventional Czochralski method in the conditions of low axial and radial thermal gradients ($\Delta T/\Delta x$ < 1.0 °C/cm). The melting temperature for Eu:

NGW is 1253 °C. The initial compounds were Na_2CO_3, WO_3, Gd_2O_3 and Eu_2O_3 (4N purity, Sigma-Aldrich) taken in stoichiometric composition. The Eu content in the growth charge was 2 at.%. The crystal was grown on [001]-oriented seed. The seed was oriented with X-ray diffraction (XRD).

A platinum crucible 70×120 mm in dimensions, tightly covered with an inverted funnel shaped platinum lid having a narrow tube (diameter: 15 mm), was mounted in a three-zone furnace with three temperature controllers (PIT-3). This lid served as a radiation screen and as a diffusion lock for volatile substances which prevented excessive evaporation and decomposition of the melt. The lid installation strongly reduced the thermal instabilities during the growth process. Electronic feedback was provided by a sensitive weighting system (precision of 10 mg in the 1 kg range). The pulling rate was ~2 mm / day. The growth rate in terms of crystal weight was 1 g/day in the beginning of the process and 20 g / day when the crystal diameter reached its maximum value. After separation from the melt, the crystal was cooled to room temperature at a rate of 20–30 °C/h.

The as-grown bulk (Fig. 1) had the dimensions of 30×30×65 mm^3 and it was oriented along the [001] axis, as confirmed by XRD. The bulk consisted of ~20 mm-long pyramidal part and prismatic one with a circular cross-section which was uniform over the crystal length thus indicating good control of thermal instabilities at the solid-liquid interface. The end facet of the crystal was flat corresponding to the {001} plane. As Eu:NGW crystal was grown in air atmosphere, the oxygen vacancies result in the formation of color center in the as-grown crystal, as described previously for the $NaLa(MoO_4)_2$ crystal [13]. Indeed, the as-grown Eu:NGW crystal was dark red-brown colored, as shown in Fig. 2(a). The inspection of the absorption spectrum revealed broad band spanning from ~350 to 650 nm with a maximum at ~410 nm and peak absorption of ~15 cm^{-1}. To reduce the number of these vacancies, the as-grown crystal was annealed in the air at 850±50 °C for 72 h with a slow heating and cooling (< 20 °C/h). After the annealing, the crystal became transparent with a slight yellow coloration due to Eu doping, Fig. 2(b) (the coloration of annealed undoped crystal was slightly greenish). The annealing also served for reduction of stresses in the as-grown bulk which allowed cutting of the crystal without producing additional cracks. The annealed crystal was of high optical quality. It did not contain inclusions and air bubbles, as well as cracks. The optical losses in the transparency region (at ~1 μm) were determined with the ISO-standard laser calorimetry to be $<0.5\times10^{-4}$ cm^{-1}. The Mohs' hardness of Eu:NGW is ~4.7.

Concentration of Eu^{3+} ions was determined with Energy Dispersive X-ray (EDX) spectroscopy using a Vega II LMU electron microscope equipped with an Inca Energy 350 X-ray microanalyzer. The atomic percent of Eu^{3+} in the annealed crystal was 4.9±0.3 at.% which corresponded to an absolute concentration $N_{Eu} = 3.1\pm0.2\times10^{20}$ cm^{-3} (density of the crystal measured by the hydrostatic method was $\rho = 7.15$ g/cm^3). Thus, the segregation coefficient for Eu^{3+} ions was $K = [Eu]_{crystal}/[Eu]_{melt} = 2.45 \pm 0.05$. The stoichiometric formula for the studied crystal was $NaGd_{0.951}Eu_{0.049}(WO_4)_2$.

The structure of the Eu:NGW crystal (tetragonal, space group $I4_1/a$) was confirmed with XRD. The unit cell parameters for the 4.9 at.% Eu:NGW are $a = b = 5.262$ Å and $c = 11.389$ Å (number of formula units per unit cell, $Z = 2$) which are slightly larger than the parameters for undoped NGW crystal with $a = b = 5.240$ Å and $c = 11.368$ Å. This agrees with the fact that ionic radius of Eu^{3+} is larger than that of Gd^{3+}. The unit cell volume for Eu:NGW crystal is $V = 315.4$ $Å^3$ and the calculated density is 7.119 g/cm^3 which agrees with the experimental value. Thermal expansion of Eu:NGW crystal was studied in the temperature range of 20–200 °C with a horizontal dilatometer Netzsch

402PC. The resulted values are $\alpha_a = 9.0$ and $\alpha_c = 19.1\times10^{-6}$ K^{-1}, and the anisotropy degree is $\alpha_c/\alpha_a = 2.1$. The volumetric thermal expansion is equal to $\alpha_{vol} = 2\alpha_a + \alpha_c = 37.1\times10^{-6}$ K^{-1}.

3. Experimental

From the annealed Eu:NGW, the 3 mm-thick plates were cut and polished for spectroscopic study with respect to the [100] and [001] axes. Eu:NGW is a negative uniaxial crystal. Its optical axis is parallel to the [001]-axis. The refractive indices of undoped NGW crystal are $n_o = 1.945$ and $n_e = 1.935$ at ~1 μm [2]. The prepared samples provided access to polarizations $E \parallel a$ (σ-polarization) and $E \parallel c$ (π-polarization).

Room-temperature (RT) absorption spectrum of Eu:NGW was measured with Varian CARY-5000 spectrophotometer. In the visible and UV ranges (300...650 nm), the spectral bandwidth (SBW) was 0.02 nm and in the near-IR (1.8...2.8 μm), the value was SBW = 0.1 nm. Absorption cross-section was calculated from the absorption coefficient, $\sigma_{abs} = \alpha/N_{Eu}$. For low-temperature (LT) measurements at 6 K, we used an Oxford Instruments Ltd. cryostat (SU 12 model) with helium-gas close-cycle flow.

Photoluminescence (PL) of Eu:NGW was excited at 355 nm. The spectrum was measured with a lock-in amplifier, monochromator MDR-23 (SBW = 0.2 nm) and a sensitive Hamamatsu C5460-01 photodetector. Glan-Taylor prism was used to separate the $E \parallel a$ and $E \parallel c$ polarization states of emission. Spectral sensitivity of the set-up was determined with a halogen lamp with a calibrated spectral power density.

For time-resolved PL studies, ns optical parametric oscillator Lotis TII LT-2214 tuned to 530 nm was used as excitation source. The decay curves were detected with monochromator MDR-12 (SBW = 1 nm), fast Hamamatsu C5460 photodetector (response time, 40 ns) and a 500 MHz Textronix TDS-3052B digital oscilloscope. The decay from $^5D_0$ state was monitored at 610 nm and 700 nm, and the characteristic decay time was determined according to a single-exponential law, $I_{PL} = I_0\exp(-t/\tau)$.

Raman spectra were measured using a Renishaw inVia Raman microscope with a x50 objective. The excitation wavelength was 632.8 nm (He–Ne laser). The spectral resolution was 0.1 cm^{-1}.

4. Optical spectroscopy

Optical absorption spectrum of the Eu:NGW crystal is shown in Fig 3 (light polarization is $E \parallel a$, RT). The absorption band attribution is performed according to earlier results [36]. The feature of Eu^{3+} ion is a small energy gap between the ground state ($^7F_0$) and the lower-lying excited state ($^7F_1$), ~350 cm^{-1} in DTs. The latter manifold is thermally populated at RT (the fractional population probabilities for $^7F_0$ and $^7F_1$ states are ~0.65 and 0.33, respectively, as estimated from Boltzmann distribution). Indeed, in the absorption spectrum the transitions from both $^7F_0$ and $^7F_1$ states are detected. In the near-IR, characteristic bands of Eu^{3+} ions related to the transitions $^7F_{0,1} \rightarrow {}^7F_5$ (3500-3900 cm^{-1}) and $^7F_6$ (4500-5200 cm^{-1}) are observed. In the visible, intense absorption bands are related to the transitions to the higher-lying $^5D_0$ (~16800 cm^{-1}), $^5D_1$ (~18350 cm^{-1}), $^5D_2$ (~21500 cm^{-1}), $^5D_3$ (~24700 cm^{-1}) and $^5L_6$ multiplets (~25350 cm^{-1}). For wavenumbers above 25500 cm^{-1}, energy sublevels from the ^5L_J, ^5G_J and ^5D_J multiplets are partially overlapped and their attribution is complicated.

The UV absorption edge of the Eu:NGW crystal is at $\lambda_{UV} = 325$ nm (E_g ~3.8 eV) and it is almost independent from the polarization, as determined from the Tauc plot. This determines smaller

transparency region of NGW in UV as compared with monoclinic KGW crystal with λ_{UV} = 290 nm. This is typical for all tetragonal DTs and DMos and causes weak yellow-green coloration of undoped samples, while undoped monoclinic DTs are clear.

The details of absorption bands of Eu:NGW crystal related to the transitions $^7F_{0,1} \rightarrow {}^5L_6$, $^5D_3$ and $^5D_2$ (blue region) and $^7F_{0,1} \rightarrow {}^5D_1$ (green region) are analyzed in Fig. 4 at RT and LT (light polarization $E \parallel a$). For LT, the spectra are shown in a.u. The UV pumping of Eu-doped DT typically causes the color center formation and darkening of the sample that can prevent laser operation [35]. Thus, only the absorption bands in the visible will be considered.

The intense band peaked at 394.5 nm ($\sigma_{abs} = 1.9\times10^{-20}$ cm^2) is ascribed to the $^7F_0 \rightarrow {}^5L_6$ transition. It can be used for pumping of Eu:NGW by blue InGaN laser diodes emitting in the vicinity of ~400 nm. The full width at half maximum (FWHM) for this band is 0.8 nm which is almost 3 times larger than that of monoclinic Eu:KGW [37]. The feature of Eu:NGW is the anomalously strong absorption at 400-420 nm which is attributed to the $^7F_{0,1} \rightarrow {}^5D_3$ transitions. Second relevant band in the blue contains two very narrow (FWHM ≈0.3 nm) peaks at 465.0 and 465.4 nm (for $E \parallel a$, while for $E \parallel c$ only second peak is detected) and the maximum σ_{abs} is 1.3×10^{-20} cm^2 at 465.4 nm. Eu:NGW can be pumped into this band by a frequency-doubled optically pumped semiconductror lasers. The band, related to the transition $^7F_1 \rightarrow {}^5D_1$, was previously used for pumping of Eu^{3+}-doped monoclinic DT with green frequency-doubled Nd lasers [24,33]. This band is determined by broad local peak at 535.5 nm with $\sigma_{abs} = 1.2\times10^{-21}$ cm^2 and FWHM = 3.1 nm. The weaker band related to $^7F_0 \rightarrow {}^5D_1$ transition contains local peaks at 526.7 and 529.8 nm and demonstrates small FWHM, <0.4 nm, so it is not suitable for pumping.

The comparison of peak absorption cross-sections of Eu^{3+} ions related to the $^7F_1 \rightarrow {}^5D_1$ transition in Eu^{3+}-doped DT is presented in Table 1. Monoclinic DT offer one order of magnitude higher σ_{abs} (as compared with Eu:NGW) which is attributed to their low-symmetry structure. However, FWHM of the absorption band for Eu:NGW is 6 times larger than that for monoclinic DT [38] which can reduce the requirements for pump wavelength. The latter factor strongly reduced efficiency of Eu lasers based on monoclinic crystals [33,34]. In particular, for 20 mm-long 5 at.% Eu:NGW, absorption at ~534 nm is ~35%. Further improvement of pump efficiency for Eu:NGW can be done by growing of highly doped (>20 at.% Eu) crystals. This is possible due to the closeness of ionic radii of Gd^{3+} and Eu^{3+} (moreover, the stoichiometric $NaEu(WO_4)_2$ crystal can exist in the tetragonal phase [39]).

Photoluminescence (PL) of Eu:NGW crystal was excited in the UV at 355 nm. The used excitation wavelength allowed population of metastable $^5D_0$ and higher-lying $^5D_1$, $^5D_2$ and $^5D_3$ states. For these multiplets, in contrast to the $^5D_0$ one, the energy gap to the lower-lying state is relatively small (~1000-2000 cm^{-1}) which, however, is enough wide to prevent domination of multi- phonon non-radiative relaxation over the radiative transitions and, hence, the emission from these states is observed. The PL spectrum of Eu:NGW is shown in Fig. 5 together with the interpretation of observed emission bands related to the $^5D_J \rightarrow {}^7F_{J'}$ (shortly J → J') transitions. The bands with the maxima at ~580, 595, 614, 645, 700, 745 and 780 nm are related with the 0 → 0', 1', 2', 3', 4', 5' and 6' transitions, respectively. The most intense band is at ~614 nm (0 → 2') and it determines red color of the PL. CIE 1931 (*Commission internationale de l'éclairage*) coordinates for PL of Eu:NGW crystal are x = 0.671 and y = 0.329. The dominant wavelength in the emission spectrum is λ_d = 608 nm with the

purity p = 99%. A comparison of color coordinates of PL from single- and nano-crystalline Eu-doped DT and DMo is presented in Table 2.

It should be noted that no signs of blue Eu^{2+} emission were detected for Eu:NGW crystals (both as-grown and annealed). Thus, we conclude that all Eu ions in the NGW crystal are trivalent.

Eu^{3+} is known for its hyper-sensitive purely electric-dipole, ED, transition $^5D_0 \rightarrow {}^7F_2$ that is the indicator of the symmetry of the ion site. If the site has no inversion center, this transition will be dominant over the $^5D_0 \rightarrow {}^7F_1$ magnetic dipole, MD, one [18,43]. The ratio of integral intensities of the above mentioned emission bands, is called the asymmetry parameter R [44]:

$$R = \frac{I_{ED}(^5D_0 \rightarrow {}^7F_2)}{I_{MD}(^5D_0 \rightarrow {}^7F_1)}. \quad (1)$$

For Eu:NGW, R = 3.4 (a prevalence of ED transition). This is consistent with the fact that Eu^{3+} ions replaces Gd^{3+} ones located in distorted S_4 sites without inversion center. The value of R for Eu:NGW is lower than for Eu:KGW ($R \approx 10$) [37] as in the latter case Eu^{3+} ions are located in the C_2 sites with lower symmetry.

The PL decay curves for Eu:NGW crystal are shown in Fig. 6. The measurements were performed for the $^5D_0 \rightarrow {}^7F_2$ (at 610 nm) and $^5D_0 \rightarrow {}^7F_4$ (700 nm) emission channels. The decay curves are clearly single-exponential. The luminescence decay time τ is equal to 480±10 μs. A comparison of decay times for Eu^{3+} emission in DT and DMo is presented in Table 3. The value of τ for Eu:NGW is similar to that of monoclinic DT (430...510 μs) [37,38]. For Eu-doped DT and DMo nanopowders, wider range of decay times was reported, from ~0.5 to ~1 ms, depending on the crystal composition and Eu doping level (cf. Table 3).

To calculate the stimulated-emission (SE) cross-sections, σ_{SE}, for Eu:NGW we have used the Füchtbauer–Ladenburg (F-L) equation [48]:

$$\sigma_{SE}^{i}(\lambda) = \frac{\lambda^5}{8\pi n_i^2 \tau c} \frac{W_i(\lambda)}{1/3 \sum_{i=a,a,c} \int \lambda W_i(\lambda) d\lambda}. \quad (2)$$

Here, $W_i(\lambda)$ is the measured spectral power density of luminescence for $E \parallel a$ and $E \parallel c$ oscillation states, λ is the light wavelength, n_i is the refractive index corresponding to i-th polarization, τ is the lifetime of the emitting state ($^5D_0$ level of Eu^{3+}), c is the speed of light, and averaging is performed as $1/3(2\int_a + \int_c)$ where $\int$ is the integrated luminescence power density. This is related to the fact as for Eu:NGW, light polarization along [100] and [010] axes are identical (both corresponds to $E \parallel a$ polarization).

The results on SE cross-sections for Eu:NGW crystal are shown in Fig. 7. For $^5D_0 \rightarrow {}^7F_4$ transition (deep-red emission), the peak σ_{SE} values are very similar for light polarizations $E \parallel a$ and $E \parallel c$, ~1.5×10^{-21} cm^2. The peak wavelengths λ_{peak} are 697.2 and 698.3 nm, respectively. These values are much lower than that for monoclinic Eu:DT (cf. Table 4). In addition, λ_{peak} for Eu:NGW is also shorter: for Eu:KGW, laser operation was achieved at ~702 nm. For the $^5D_0 \rightarrow {}^7F_2$ transition (red emission), the anisotropy of SE cross-sections is more profound. For light polarization $E \parallel a$, the spectrum contains intense peak centered at 610.9 nm with $\sigma_{SE} = 1.08\times10^{-20}$ cm^2. For $E \parallel c$, this emission band splits to two components peaked at 607.9 nm and 610.9 nm and the maximum $\sigma_{SE} = 0.51\times10^{-20}$ cm^2. The anisotropy degree for this transition is $\sigma_{SE}(a):\sigma_{SE}(c) \approx 2:1$. Thus, for this transition, the linearly polarized laser output is expected.

The study of spectroscopic properties of Eu:NGW indicates that both principal light polarizations, $E \parallel a$ and $E \parallel c$, can be useful for potential laser applications. To access both of them, the crystal should be cut perpendicular to the [001] axis which is usually denoted as *a*-cut. In addition, for NGW, particularly this crystal cut is beneficial in terms of weaker thermo-optic effects [49].

Both monoclinic and tetragonal DTs are well-known Raman-active media [50,51] also offering the possibility of self-Raman conversion [52]. Raman spectra of Eu:NGW are shown in Fig. 8 for *a*(*bb*)*a*, *a*(*bc*)*a* and *a*(*cc*)*a* geometries. The strongest Raman peak of the stretching vibration of the $(WO_4)_2^-$ anion, the $v_1(A_g)$ mode according to the scheelite $I4_1/a$ symmetry, is centered at 916 cm^{-1} and its bandwidth is ~23 cm^{-1}. Raman spectra are strongly polarized; for an *a*-cut crystal, polarization $E \parallel c$ is of interest for Raman conversion. The assignment of Raman active modes for Eu:NGW crystal is presented in Table 5, in accordance with [51].

Further work on Eu^{3+}-doped sodium DT should be focused on growth of highly-doped (>20 at.% Eu) NGW crystals and laser operation in the deep-red (~698 nm) and red (~611 nm) spectral regions. The use of different "passive" ions like La^{3+} or Bi^{3+} can induce the transition cross-section increase and, thus, the study of Eu:NRW crystals with R = Y, Lu, La or Bi or Eu:NaRMo crystals seems to be very interesting. The growth of Eu^{3+}-doped sodium DT along the [100] direction can be useful for preparation of long *a*-cut laser elements.

5. Conclusion

We report on Czochralski growth and spectroscopic study of tetragonal Eu^{3+}-doped sodium double tungstate, $NaGd(WO_4)_2$ (Eu:NGW). By providing low axial and radial temperature gradients (< 1.0 °C/cm) we were able to stabilize the growth process and produce large-volume bulk of very high optical quality. The Eu doping concentration was as high as 4.9 at.% but the results indicate good prospects for growing of highly-doped Eu:NGW crystals. In addition, annealing in air was found to be crucial to diminish the oxygen vacancies resulting in dark red-brown coloration of the as-grown bulk.

Although absorption and stimulated-emission cross-sections for Eu^{3+} ions in NGW are lower than those of Eu^{3+}-doped monoclinic double tungstates, Eu:NGW offers wider absorption bands which can be favorable for increased pump efficiency. In particular, for the transition $^7F_1 \rightarrow {}^5D_1$ which can be used for pumping with green frequency-doubled Nd lasers, $\sigma_{abs} = 1.2\times10^{-21}$ cm^2 at 535.5 nm while FWHM of the corresponding absorption band is 3.1 nm. In the deep-red region, the laser operation with Eu:NGW is expected at ~698 nm and the corresponding stimulated-emission cross- section is $\sigma_{SE} = 1.6\times10^{-21}$ cm^2 (at RT, for $E \parallel c$ polarization). Under UV excitation at 355 nm, Eu:NGW provides intense red emission with color coordinates $x = 0.671$, $y = 0.329$ (CIE 1931 color space).

Acknowledgements

P.L. thanks Dr. Alexey Kornienko (Vitebsk State Technological University) for fruitful discussion about the optical absorption of the Eu:NGW crystal and Dr. Vitaly Shimanski (Belarusian State University) for the help in X-ray diffraction studies.

References

1. K. A. Subbotin, E. V. Zharikov, V. A. Smirnov, Optics and Spectr. 92 (2002) 601-608.
2. C. Cascales, M. D. Serrano, F. Esteban-Betegón, C. Zaldo, R. Peters, K. Petermann, G. Huber, L. Ackermann, D. Rytz, C. Dupré, M. Rico, J. Liu, U. Griebner, V. Petrov, Phys. Rev. B 74 (2006) 174114.
3. A. A. Kaminskii, H. J. Eichler, K. Ueda, N. V. Klassen, B. S. Redkin, L. E. Li, J. Findeisen, D. Jaque, J. García-Sole, J. Fernández, R. Balda, Appl. Opt. 38 (1999) 4533-4547.
4. Yu.K. Voron'ko, K.A. Subbotin, V.E. Shukshin, D.A. Lis, S.N. Ushakov, A.V. Popov, E.V. Zharikov, Opt. Mater. 29 (2006) 246-252.
5. A. A. Kaminskii, A. Kholov, P. V. Klevtsov, S. Kh. Khafizov, Phys. stat. sol (a) 114 (1989) 713-719.
6. A. Garcia-Cortes, C. Cascales, A. de Andres, C. Zaldo, E.V. Zharikov, K.A. Subbotin, S. Bjurshagen, V. Pasiskevicius, M. Rico, IEEE J. Quantum Electron. 43 (2007) 157-167.
7. J. Liu, J. M. Cano-Torres, C. Cascales, F. Esteban-Betegón, M. D. Serrano, V. Volkov, C. Zaldo, M. Rico, U. Griebner, V. Petrov, Phys. stat. sol. (a) 202 (2005) R29-R31.
8. M. Rico, J. Liu, U. Griebner, V. Petrov, M. D. Serrano, F. Esteban-Betegón, C. Cascales, C. Zaldo, Opt. Express 12 (2004) 5362-5367.
9. J.M. Cano-Torres, M. D. Serrano, C. Zaldo, M. Rico, X. Mateos, J. Liu, U. Griebner, V. Petrov, F. J. Valle, M. Galán, G. Viera, J. Opt. Soc. Am. B 23 (2006) 2494-2502.
10. E. V. Zharikov, D. A. Lis, A. V. Popov, K. A. Subbotin, S. N. Ushakov, A. V. Shestakov, I. M. Razdobreev, Quantum Electron. 36 (2006) 515–516.
11. X. Han, F. Fusari, M. D. Serrano, A. A. Lagatsky, J. M. Cano-Torres, C. T. A. Brown, C. Zaldo, W. Sibbett, Opt. Express 18 (2010) 5413-5419.
12. P.V. Klevtsov, L.P. Kozeeva, Sov. Phys. Dokl. 14 (1969) 185.
13. G.M. Kuz'micheva, D.A. Lis, K.A. Subbotin, V.B. Rybakov, E.V. Zharikov, J. Cryst. Growth 275 (2005) e1835–e1842.
14. V. Volkov, C. Zaldo, J. Cryst. Growth 206 (1999) 60-64.
15. A. García-Cortés, J. M. Cano-Torres, X. Han, C. Cascales, C. Zaldo, X. Mateos, S. Rivier, U. Griebner, V. Petrov, F. J. Valle, J. Appl. Phys. 101 (2007) 063110.
16. A.A. Lagatsky, X. Han, M.D. Serrano, C. Cascales, C. Zaldo, S. Calvez, M.D. Dawson, J. A. Gupta, C.T.A. Brown, W. Sibbett, Opt. Lett. 35 (2010) 3027-3029.
17. G. Wakefield, E. Holland, P.J. Dobson, J.L. Hutchison, Adv. Mater. 13 (2001) 1557–1560.
18. V.V. Atuchin, A.S. Aleksandrovsky, O.D. Chimitova, T.A. Gavrilova, A.S. Krylov, M.S. Molokeev, A.S. Oreshonkov, B.G. Bazarov, J.G. Bazarova, J. Phys. Chem. C. 118 (2014) 15404-15411.
19. K.W. Meert, V.A. Morozov, A.M. Abakumov, J. Hadermann, D. Poelman, P.F. Smet, Opt. Express 22 (S3) (2014) A961-A972.
20. P. Shi, Z. Xia, M.S. Molokeev, V.V. Atuchin, Dalton Trans. 43 (2014) 9669-9676.
21. H. Ji, Z. Huang, Z. Xia, M. S. Molokeev, X. Jiang, Z. Lin, V.V. Atuchin, Dalton Trans. 44 (2015) 7679-7686.
22. E.J. Schimitschek, Appl. Phys. Lett. 3 (1963) 117–118.
23. J.H. Park, A.J. Steckl, Appl. Phys. Lett. 85 (2004) 4588–4590.
24. S.N. Bagaev, V.I. Dashkevich, V.A. Orlovich, S.M. Vatnik, A.A. Pavlyuk, A.M. Yurkin, Quantum Electron. 41 (2011) 189–192.
25. S. Neeraj, N. Kijima, A.K. Cheetham, Chem. Phys. Lett. 387 (2004) 2-6.
26. C.H. Chiu, M.F. Wang, C.S. Lee, T.M. Chen, J. Sol. State Chem. 180 (2007) 619–627.
27. L. Li, L. Liu, W. Zi, H. Yu, S. Gan, G. Ji, H. Zou, X. Xu, J. Lumin. 143 (2013) 14–20.

28. X.H. Qian, X.P. Pu, D.F. Zhang, L. Li, M.J. Li, S.T. Wu, J. Lumin. 131 (2011) 1692–1695.
29. R. Pazik, A. Zych, W. Strek, Mater. Chem. Phys. 115 (2010) 536–540.
30. L. Macalik, P.E. Tomaszewski, R. Lisiecki, J. Hanuza, J. Sol. State Chem. 131 (2008) 2591–2600.
31. M. Galceran, M.C. Pujol, P. Gluchowski, W. Strek, J.J. Carvajal, X. Mateos, M. Aguilo, F. Diaz, Opt. Mater. 32 (2010) 1493–1500.
32. X. Gao, Y. Wang, D. Wang, B. Liu, J. Lumin. 129 (2009) 840–843.
33. V.I. Dashkevich, S.N. Bagaev, V.A. Orlovich, A.A. Bui, P.A. Loiko, K.V. Yumashev, N.V. Kuleshov, S.M. Vatnik, A.A. Pavlyuk, Laser Phys. Lett. 12 (2015) 015006.
34. V.I. Dashkevich, S.N. Bagayev, V.A. Orlovich, A.A. Bui, P.A. Loiko, K.V. Yumashev, A.S. Yasukevich, N.V. Kuleshov, S.M. Vatnik, A.A. Pavlyuk, Laser Phys. Lett. 12 (2015) 085001.
35. P.A. Loiko, et al., J. Lumin. 168 (2015) 102–108.
36. W. T. Carnall, P. R. Fields, K. Rajnak, J. Chem. Phys. 49 (1968) 4450.
37. P.A. Loiko, et al., Laser Phys. 23 (2013) 105811.
38. P.A. Loiko, et al., J. Lumin. 153 (2014) 221–226.
39. Q. Shao, H. Li, K. Wu, Y. Dong, J. Jiang, J. Lumin. 129 (2009) 879–883.
40. F. Mo, L. Zhou, Q. Pang, F. Gong, Z. Liang, Ceram. Intern. 38 (2012) 6289-6294.
41. Y. Zhai, J. Li ,X. Li, Y. Dong, Y. Wang, S. Song, J. Sol-Gel Sci. Technol. 74 (2015) 544–549.
42. Y. Su, C. Du, Q. Jia, L. Lv, Q. Liu, X. Wang, J. Nanosci. Nanotechnol. 11 (2011) 9855-9860.
43. P.A. Tanner, Chem. Soc. Rev. 42 (2013) 5090-5101.
44. A.F. Kirby, F.S. Richardson, J. Phys. Chem. 87 (1983) 2544–2556.
45. B. Yan, J. Wu, J. Mater. Research 24 (2009) 32–38.
46. P. Jia, X. Liu, Y. Luo, M. Yu, J. Lin, J. Electrochem. Soc. 154 (2007) J39-J43.
47. Z. Wang, J. Zhong, H. Liang, J. Wang, Opt. Mater. Express 3 (2013) 418–425.
48. B.F. Aull, H.P. Jenssen, IEEE J. Quantum Electron. 18 (1982) 925–930.
49. P.A. Loiko, X. Han, K.V. Yumashev, N.V. Kuleshov, M. D. Serrano, C. Cascales, C. Zaldo, Appl. Phys. B. 111 (2013) 279–287.
50. T.T. Basiev, A.A. Sobol, P.G. Zverev, L.I. Ivleva, V.V. Osiko, R.C. Powell, Opt. Mater. 11 (1999) 307–314.
51. L. Macalik, J. Hanuza, A.A. Kaminskii, J. Molec. Struct. 555 (2000) 289–297.
52. A.A. Demidovich, A.S. Grabtchikov, V.A. Lisinetskii, V.N. Burakevich, V.A. Orlovich, W. Kiefer, Opt. Lett. 30 (2005) 1701–1703.

List of figure captions

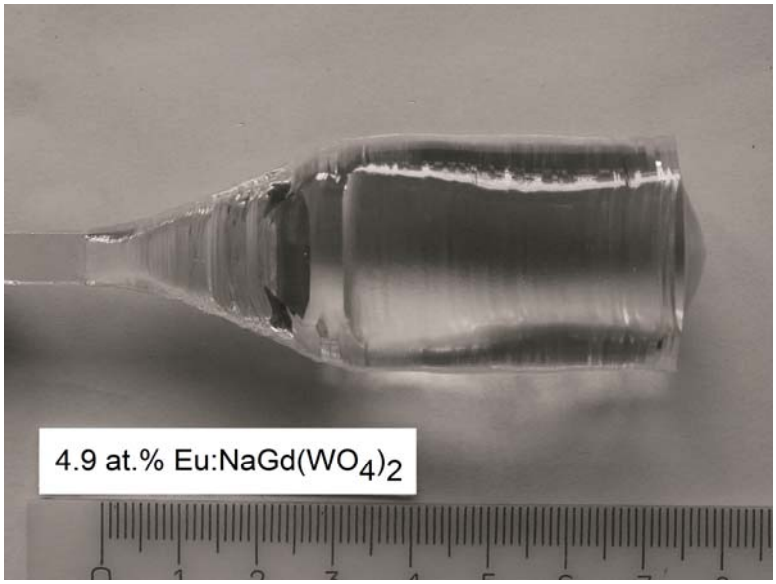

Figure 1 Image of the as-grown bulk of Eu:NGW crystal.

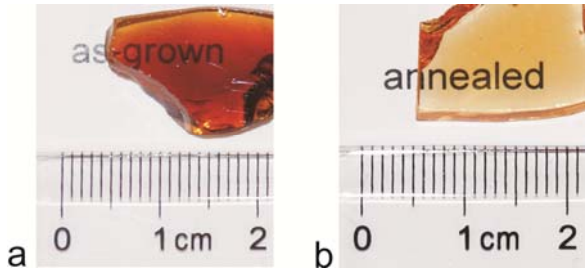

Figure 2 Images of polished plates from the as-grown crystal (a) and annealed one (b).

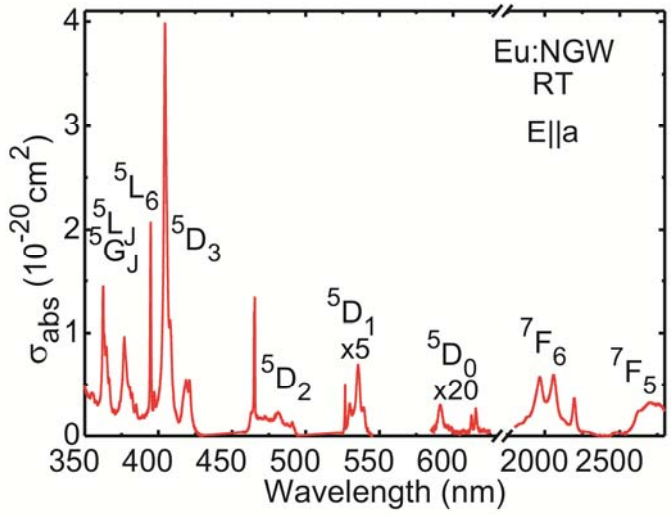

Figure 3 Absorption cross-section spectrum of Eu:NGW crystal at room-temperature, light polarization is $E \parallel a$.

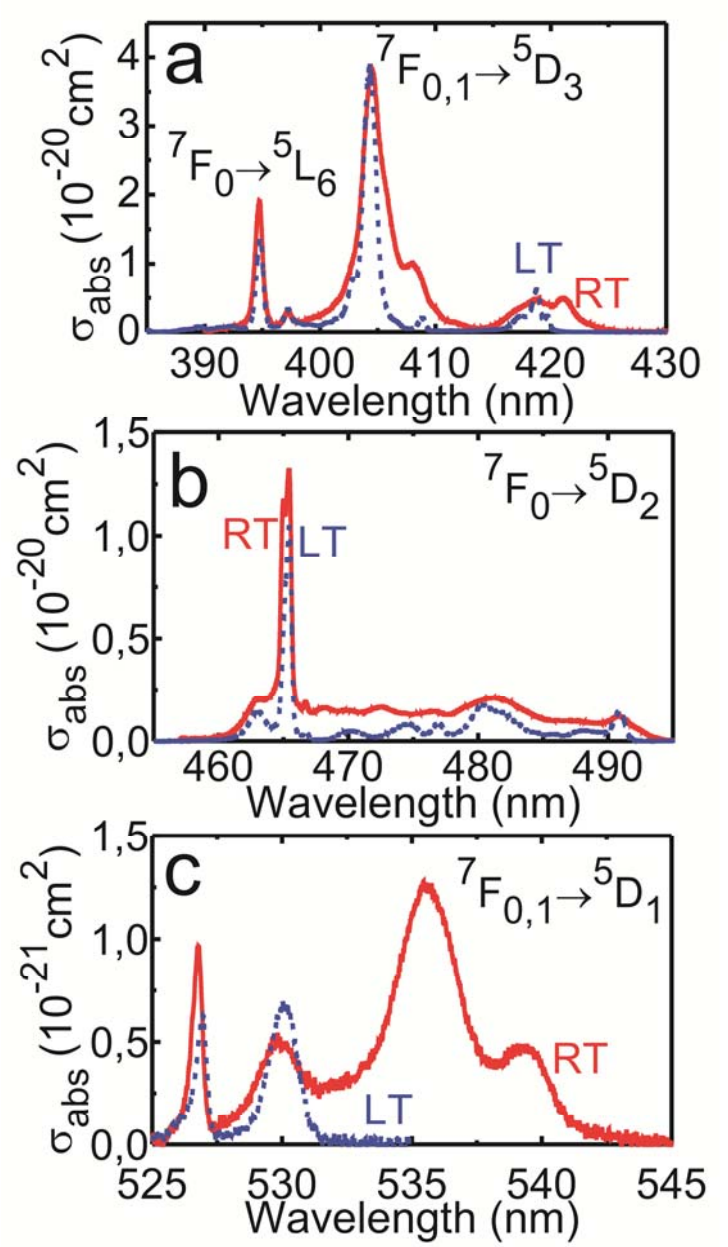

Figure 4 Details of the absorption bands related to the $^7F_{0,1} \rightarrow {}^5D_3$ and $^5L_6$ (a), $^7F_0 \rightarrow {}^5D_2$ (b) and $^7F_{0,1} \rightarrow {}^5D_1$ (c) transitions of Eu^{3+} ions in NGW crystal at room-temperature (RT) and 6 K (LT), light polarization is $E \parallel a$. The spectrum for LT is shown in a.u.

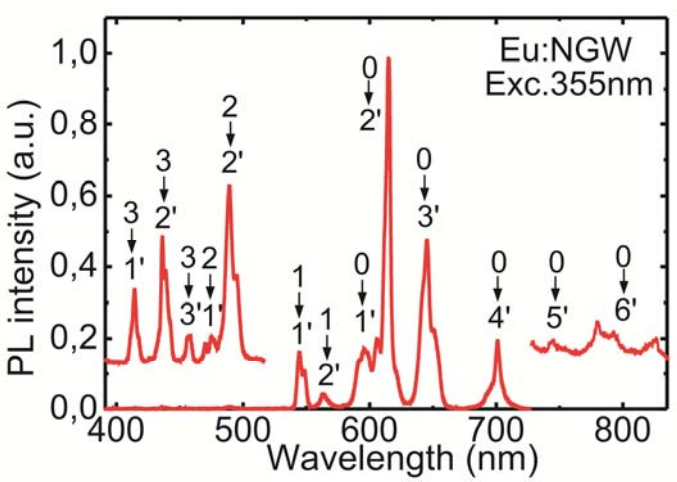

Figure 5 Photoluminescence (PL) spectrum of Eu:NGW crystal at room temperature, numbers on the graph denote $^5D_J \rightarrow {}^7F_{J'}$ (shortly J→J') transitions of Eu^{3+} ions, excitation wavelength is 355 nm.

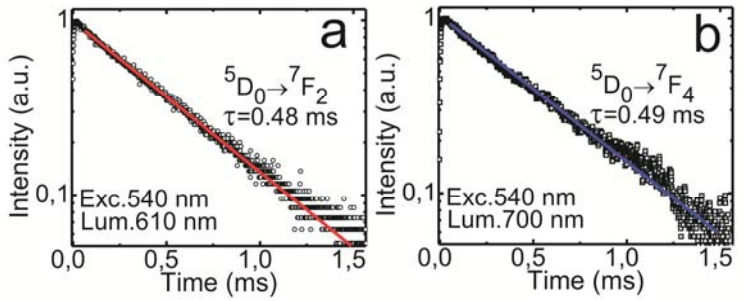

Figure 6 Decay of red luminescence of Eu^{3+} ions in NGW at 610 nm, $^5D_0 \rightarrow {}^7F_2$ transition, (a) and 702 nm, $^5D_0 \rightarrow {}^7F_4$ transition, (b); excitation wavelength is 530 nm.

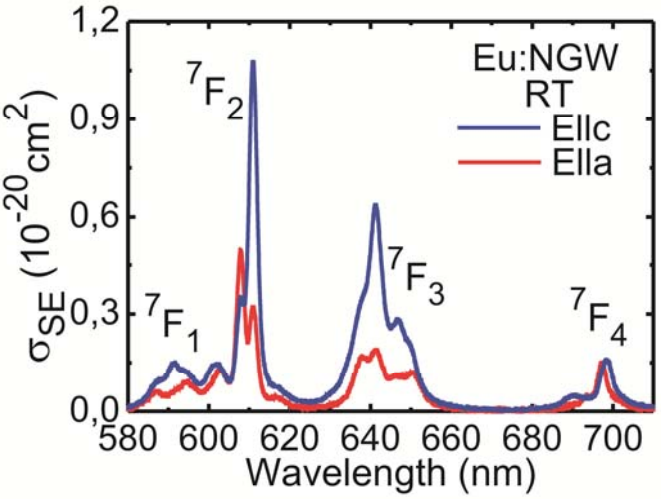

Figure 7 Stimulated-emission cross-sections (σ_{SE}) spectra of Eu:NGW crystal for light polarizations $E \parallel a$ and $E \parallel c$.

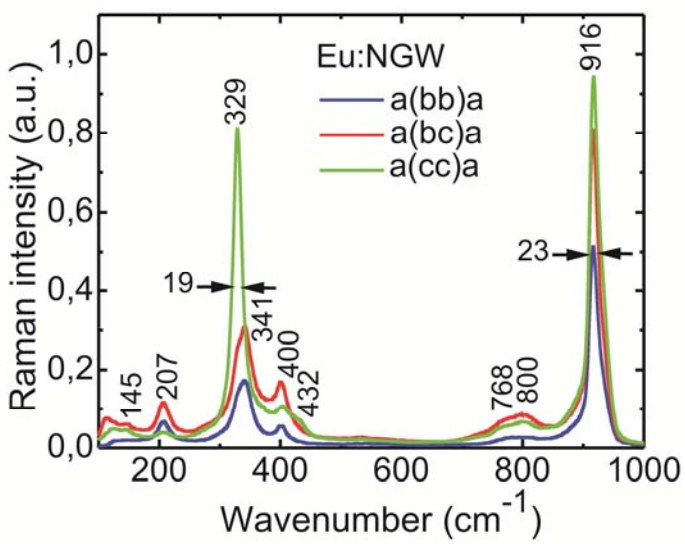

Figure 8 Polarized Raman spectra of Eu:NGW crystal for the *a*(*bb*)*a*, *a*(*bc*)*a* and *a*(*cc*)*a* geometries: excitation wavelength is 632.8 nm, *a* and *b* axes are identical for NGW.

Table 1 Peak absorption cross-sections, σ_{abs}, the corresponding wavelengths, λ_{peak}, and full widths at half maximum of the absorption peak, $\Delta\lambda$, for $^7F_1 \rightarrow {}^5D_1$ transition of Eu^{3+} ions in double tungstate crystals.

Transition	Crystal*	Polar.	λ_{peak}, nm	$\Delta\lambda$, nm	σ_{abs}, 10^{-20} cm^2
$^7F_1 \rightarrow {}^5D_1$	Eu:$NaGd(WO_4)_2$	*a*	535.5	3.08	0.12
	Eu:$KGd(WO_4)_2$	*m*	534.3	0.66	0.89
	Eu:$KY(WO_4)_2$	*m*	534.3	0.59	1.71
	Eu:$KLu(WO_4)_2$	*m*	534.2	0.66	0.95

*Results for monoclinic DT are in accordance with [35,37,38].

Table 2 Color coordinates *x*, *y* (in accordance with *Commission internationale de l'éclairage*, CIE 1931, color space) for photoluminescence of Eu^{3+}-doped DT and DMo compounds (C – single-crystal, P – nanocrystalline powder).

Compound	Form	*x*	*y*	Ref.
Tetragonal				
Eu:$NaGd(WO_4)_2$	C	0.671	0.329	This work
Eu:$NaGd(WO_4)_2$	P	0.661	0.339	[40]
Eu:$NaGd(MoO_4)_2$	P	0.664	0.335	[41]
Eu:$NaY(WO_4)_2$	P	0.570	0.350	[28]
Eu:$NaLa(WO_4)_2$	P	0.660	0.340	[41]
		0.320	0.300	[42]
Eu:$KLa(WO_4)_2$	P	0.652	0.625	[27]
Eu:$LiLa(WO_4)_2$	P	0.649	0.349	[27]
Monoclinic				
Eu:$KGd(WO_4)_2$	C	0.664	0.336	[37]
Eu:$KY(WO_4)_2$	C	0.670	0.329	[38]
Eu:$KLu(WO_4)_2$	C	0.672	0.328	[35]

Table 3 Lifetime of the $^5D_0$ emitting state of Eu^{3+} ions in DT and DMo compounds (C – single-crystal, P – nanocrystalline powder).

Crystal	Form	$\tau(^5D_0)$, ms	Ref.
tetragonal			
Eu:$NaGd(WO_4)_2$	C	0.49	This work
	P	0.58	[27]
Eu:$NaGd(MoO_4)_2$	P	0.57	[45]
Eu:$NaY(WO_4)_2$	P	0.5–0.7	[28,40,46]
Eu:$NaLu(MoO_4)_2$	P	0.54	[47]
Eu:$NaLu(WO_4)_2$	P	0.57	[27,47]
Eu:$NaLa(WO_4)_2$	P	0.6–1.1	[27,43]
Eu:$KLa(WO_4)_2$	P	0.65	[27]
Eu:$LiLa(WO_4)_2$	P	0.63	[27]
monoclinic			
Eu:$KGd(WO_4)_2$	C	0.51	[37]
Eu:$KY(WO_4)_2$	C	0.43	[38]
Eu:$KLu(WO_4)_2$	C	0.45	[35]

Table 4 Peak stimulated-emission cross-sections, σ_{SE}, the corresponding wavelengths, λ_{peak}, for $^5D_0 \rightarrow {}^7F_2$ and $^7F_4$ transition of Eu^{3+} ions in double tungstate crystals.

Transition	Crystal*	Polar.	λ_{peak}, nm	σ_{SE}, 10^{-20} cm^2
$^5D_0 \rightarrow {}^7F_2$	Eu:$NaGd(WO_4)_2$	*c*	610.9	1.08
	Eu:$KGd(WO_4)_2$	*m*	613.6	2.78
	Eu:$KY(WO_4)_2$	*m*	613.4	4.02
	Eu:$KLu(WO_4)_2$	*m*	613.7	3.95
$^5D_0 \rightarrow {}^7F_4$	Eu:$NGd(WO_4)_2$	*c*	698.3	0.16
	Eu:$KGd(WO_4)_2$	*m*	702.1	3.02
	Eu:$KY(WO_4)_2$	*m*	702.6	1.34
	Eu:$KLu(WO_4)_2$	*m*	703.5	1.78

*Results for monoclinic DT are in accordance with [35,37,38].

Table 5 Assignment of Raman active modes for Eu:NaGdW crystal.

Mode*, cm^{-1}			Assignment**
a(*bb*)*a*	*a*(*bc*)*a*	*a*(*cc*)*a*	
916 s	916 s	916 s	$\nu_s(WO_4)$
800 w	800 w	800 w	$\nu_{as}(WO_4)$
768 w	768 w	768 w	
		432 w	–
400 w	400 m	400 w	$\delta_{as}(WO_4)$
341 m	341 m	329 s	$\delta_s(WO_4)$
207 w	207 m	207 w	$L(WO_4)$
	145 w	145 w	$T'(Na^+/Gd^{3+})$
125 w	114 w	125 w	$T'(WO_4)$

*s – strong, m – medium, w – weak.

**ν_s, ν_{as} – stretching modes; δ_s, δ_{as} – bending modes; L – librational modes; T' –translational modes.